Temperature, pH, and Solvent Isotope Dependent Properties of the Active Sites of Resting-State and Cyanide-Ligated Recombinant Cytochrome *c* Peroxidase (H52L) Revealed by Proton Hyperfine Resonance Spectra†

James D. Satterlee,*,‡ Marina I. Savenkova,‡ Miriam Foshay,§ and James E. Erman§

Department of Chemistry, Washington State University, Pullman, Washington 99164-4630, and Department of Chemistry and Biochemistry, Northern Illinois University, De Kalb, Illinois 60115

Received April 22, 2003; Revised Manuscript Received July 15, 2003

ABSTRACT: Comparative proton NMR studies have been carried out on high-spin and low-spin forms of recombinant native cytochrome *c* peroxidase (rCcP) and its His52 → Leu variant. Proton NMR spectra of rCcP(H52L) (high spin) and rCcP(H52L)CN (low spin) reveal the presence of multiple enzyme forms in solution, whereas only single enzyme forms are found in spectra of wild-type and recombinant wild-type CcP and CcPCN near neutral pH. The spectroscopic behaviors of these forms have been studied in detail when pH, temperature, and solvent isotope composition were varied. For resting-state rCcP(H52L) the comparatively large NMR line widths compromise resolution, but two specific enzyme forms were found. They were interconvertible on the basis of varying temperature. For rCcP(H52L)CN four magnetically distinct enzyme forms were identified by NMR. It was found that these forms dynamically interconvert with changing pH, temperature, and solvent isotope composition (percent D_2O). These studies have identified the alkaline titration of His52 and essentially identical alkaline enzyme forms for natWTCcPCN and rCcP(H52L)CN. From this work we interpret an essential role of His52 in CcP function to be preservation of a single active site structure in addition to the critical role of general base catalysis.

Cytochrome *c* peroxidase from *Saccharomyces cerevisiae* (EC 1.11.1.5, CcP)[1] catalyzes the reduction of hydrogen peroxide to water using reducing equivalents supplied by two molecules of reduced cytochrome *c*, as represented by the overall reaction shown in eq 1 (*1*−*6*). Its physiological

$$H_2O_2 + 2\text{Cyt}c(Fe^{2+}) + 2H^+ \xrightarrow{\text{CcP}} 2\text{Cyt}c(Fe^{3+}) + 2H_2O \quad (1)$$

role has been presumed to be protection from H_2O_2 cytotoxicity, but it has recently been suggested that CcP could also participate in oxidative stress signaling (*7*).

Studies combining protein engineering and physical methods have revealed intimate details of the CcP enzymatic mechanism (e.g., refs *2* and *8*−*22*). For example, kinetic investigations (*10*−*12*, *20*, *24*−*26*), including those described in the accompanying paper (*27*), have established the essential fact that His52 is absolutely required for normal enzyme function. His52 mutation dramatically affects the rate of the initial reaction between CcP and H_2O_2 (*10*, *11*, *22*, *27*). His52, located in the heme active site (Figure 1), is situated close to the heme ligand binding site (*28*). In this position it structurally resembles the "distal histidine" of the globins and is strategically located to interact with hydrogen peroxide and other heme ligands. If His52 is substituted by Leu [rCcP(H52L); Figure 1D], the bimolecular rate constant for the initial hydrogen peroxide reaction falls by $\sim 10^5$, making the enzyme no more reactive toward hydrogen peroxide than heme globins (*10*, *11*). In this respect, rCcP(H52L) has lost one of the most unique of the peroxidase characteristics.

In the CcP mechanism (*2*, *8*, *28*, *29*) the initial oxidation is a bimolecular reaction of resting-state CcP with H_2O_2 (eq

† J.D.S. acknowledges support for this research from the National Institutes of Health (GM 47645). J.E.E. acknowledges support from the National Science Foundation (MCB-9513047) and the National Institutes of Health (R15 GM59740). The WSU NMR Center equipment is supported by NIH Grants RR0631401 and RR12948, NSF Grants CHE-9115282 and DBI-9604689, and the Murdoch Charitable Trust.

* Address correspondence to this author. Phone: 509-335-8620. Fax: 509-335-8867. E-mail: hemeteam@wsu.edu.

‡ Washington State University.

§ Northern Illinois University.

[1] Abbreviations: CcP, generic abbreviation for native wild-type and recombinant native wild-type cytochrome *c* peroxidase and usually implies the high-spin, resting-state form of the enzyme; natWTCcP, specifically resting-state wild-type enzyme isolated from yeast; rCcP, recombinant form of resting-state cytochrome *c* peroxidase with the exact 294 amino acid sequence of the yeast-isolated wild-type enzyme, formerly called recNATCcP (*28*); rCcP(H52L), recombinant form of CcP, with the exact 294 amino acid sequence of the yeast-isolated wild-type enzyme, in which His52 has been replaced by Leu52; CcP(MI) and CcP(MI,H52L), earlier forms of the recombinant proteins where MI indicates the presence of a Met-Ile N-terminal extension and the presence of two mutations, T53I and D152G; CcPCN, generic abbreviation for low-spin, cyanide-ligated, native wild-type and recombinant native wild-type cytochrome *c* peroxidase, a general notation throughout, where suffix "CN" attached to any CcP abbreviation indicates formation of the low-spin cyanide-ligated form; HRP, resting-state, native wild-type, high-spin horseradish peroxidase; HRPCN, resting-state, native wild-type, cyanide-ligated, low-spin horseradish peroxidase; Kan, kanamycin; Amp, ampicillin; δ-ALA, δ-aminolevulinic acid; 1D, one dimensional; 2D, two dimensional; LBB-I and -II, Washington State University Laboratory for Biotechnology and Bioanalysis, units I and II, respectively; PAGE, polyacrylamide gel electrophoresis; MALDI-TOF, matrix-assisted laser desorption ionization−time-of-flight mass spectrometry.

10.1021/bi034633c CCC: $25.00
Published on Web 08/20/2003

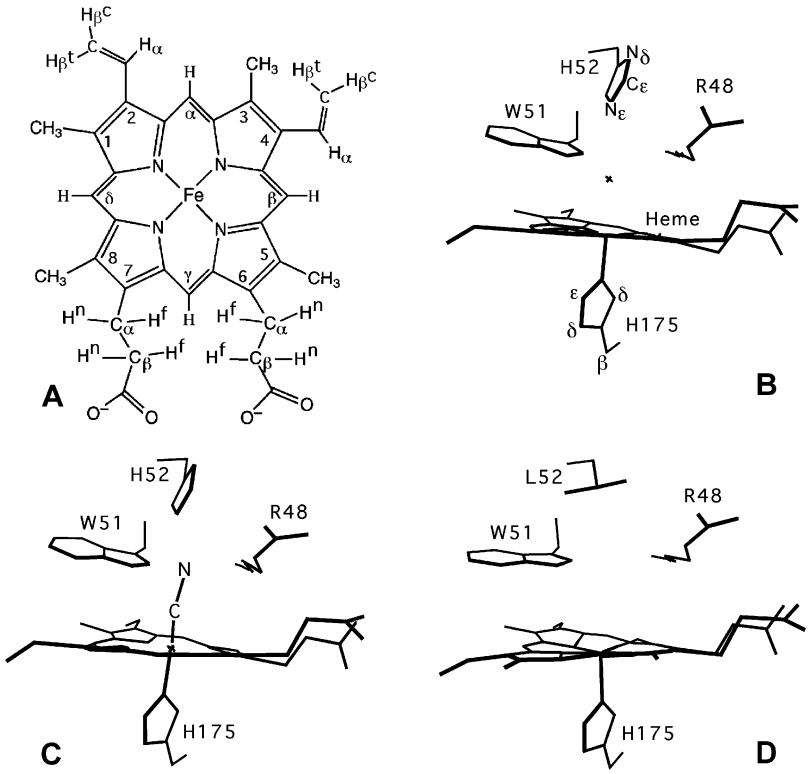

FIGURE 1: (A) Heme *b* with Fischer labeling system. Vinyl group β protons are labeled as cis (c) or trans (t) to the α proton. Propionate methylene protons are labeled stereospecifically as being either near to (n) or far from (f) the nearest heme methyl group. (B) Heme active site structure of natWTCcP (PDB identification code 2CYP; *27*). (C) Heme active site structure of natWTCcPCN. (D) Heme active site structure of rCcP(H52L) (PDB identification code 5CCP; *10*).

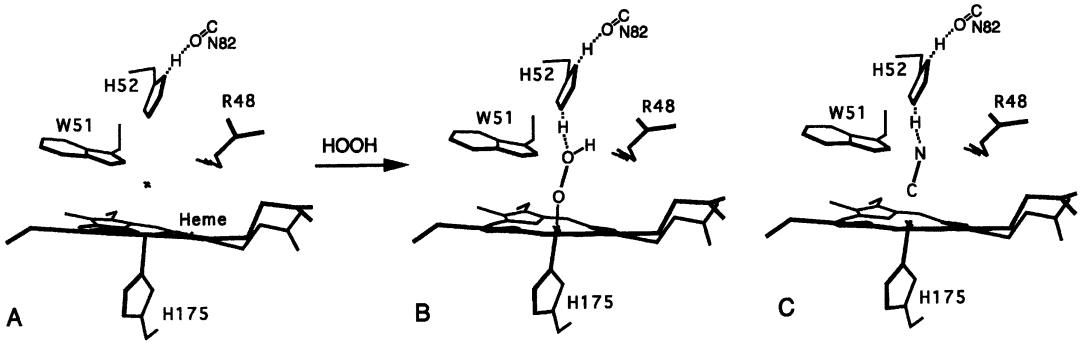

FIGURE 2: (A) Edited heme active site structure of resting-state natWTCcP explicitly showing hydrogen bonding between His52 and Asn82 (PDB identification code 2CYP; *27*). (B) Hypothetical heme active site structure of the initial reaction between CcP and the hydrogen peroxide/ES complex. This structure is modeled on the coordinates of the natWTCcPCN active site structure, shown in (C). Together, (A) and (B) provide a hypothetical view of the peroxidase initial bimolecular reaction to form ES.

2). This is a combination of a ligand binding reaction to

$$\mathrm{CcP(Fe^{3+})} + \mathrm{HOOH} \rightarrow [\mathrm{CcP{-}HOOH\ (\text{“}CcP{-}ES\text{”})}] \rightarrow \mathrm{CcP{-}I} + \mathrm{H_2O} \quad (2)$$

form the transient intermediate, CcP−ES, followed by reaction to form the first oxidized intermediate, CcP−I. Panels A and B of Figure 2 present a hypothetical model of CcP−ES based on the CcPCN coordinates (represented in Figure 1C). Figure 2C is the CcPCN structure edited to explicitly depict the His52 hydrogen-bonding role. The plausibility of our CcP−ES model rests on (i) kinetic similarities between reaction 2 and the reaction between CcP and HCN (*20*, *21*, *27*, *29*), (ii) the likelihood of similar spatial arrangement of the heavy atoms in the two structures, O−O in Figure 2B and C−N in Figure 2C, and (iii) the chemical evidence for the presence of similar His52 hydrogen bonds in CcP−ES and CcP−CN (*10*, *11*, *33*, *34*).

To further clarify chemistry related to His52 within the CcP active site, we have undertaken a comparative proton NMR study of the resting- and CN-ligated states of yeast-isolated, native wild-type CcP (natWTCcP), recombinant native wild-type CcP (rCcP; *30*), and the recombinant His52 → Leu variant [rCcP(H52L)]. HCN binding has been used as a surrogate for H_2O_2 binding due to similarities of the two reactions (*20*, *21*, *29*), as described in the accompanying paper (*27*). Also, no structure, or NMR spectrum, of the transient intermediate CcP−ES has been published because it is metastable, whereas CcP−CN is stable and well studied by NMR (*31*−*36*).

The work presented here reveals that the His52 → Leu mutation introduces an interesting diversity into the enzyme

active site that is revealed by solution ^{1}H NMR studies. Extensive diversity, or heterogeneity, has not been previously reported by X-ray crystallography (*10*) or kinetics studies (*10*, *11*) for His52 variants of CcP. Raman studies (*15*) have detected spectral heterogeneity for a His52 variant (vide infra), but the source, extent, and implications of the phenomenon were not explored. In contrast, proton NMR data for rCcP(H52L) and rCcP(H52L)CN clearly establish the simultaneous presence of multiple, magnetically distinguishable, interconverting enzyme forms in solution. Equilibrium populations of these forms depend on the solvent isotope composition (percent D), pH, and temperature. In rCcPCN it has also been possible to document pH-dependent behavior specific to His52 that is different from the pH behavior for horseradish peroxidase (*37*).

EXPERIMENTAL PROCEDURES

Unless otherwise specified all chemicals were the highest available grades and were predominantly purchased from Sigma or Fisher Scientific. Recombinant CcP with a primary sequence identical to the native yeast isolated enzyme, natWTCcP (*1*, *2*, *6*, *28*, *30*), was the gene product that constitutes rCcP and from which the gene for rCcP(H52L) was made. A plasmid, pT7CCPZf1, harboring a CcP gene with this native sequence, with T53 and D152, was obtained from Prof. Thomas Poulos (University of California, Irvine). The expressed enzymes contained no N-terminal alterations from the primary sequence of natWTCcP. Expressions in *Escherichia coli* strain BL21(DE3) were carried out with this CcP gene in pT7CCPZf1, as received and with the gene cloned into the pET24(a)+ plasmid with *Nde*I and *Eco*RI. A uniform general procedure for isolating pure enzymes was used and is described in detail elsewhere (*30*).

Both recombinant enzymes produced in this work migrated (identically to yeast-isolated natWTCcP) as single lines on SDS−PAGE, which was carried out using a PhastSystem (Pharmacia Biotech) with PhastGel homogeneous-12.5 gels (12.5% polyacrylamide gels). UV−visible spectroscopy was carried out using a GBC Cintra 40 spectrometer. DNA sequencing employed an Applied Biosystems 373 fluorescence DNA automated sequencer in the WSU LBB-I. Mass determinations were achieved using matrix-assisted laser desorption ionization−time-of-flight spectrometry (MALDI-TOF; PerSeptive Biosystems Voyager DE-RP) in the WSU LBB-II. For MALDI-TOF the samples were desorbed/ionized from a sinapinic acid matrix (natural proton isotope abundance) with a 337 nm nitrogen laser, and both internal and external mass standards were employed for mass calibrations as previously described (*30*).

Deuterated potassium phosphate buffer salts were made from K_2HPO_4 and KH_2PO_4 (Fisher) that were carried through three consecutive cycles of 100:1 (mass/mass) dissolution in 99.9% D_2O (Isotec) followed by lyophilization. NMR samples were typically made up in solutions of 99.9% D_2O solvent containing 0.1 M potassium phosphate buffer or 0.03 M potassium nitrate (Fisher). Other solutions were made from up to 90% purified natural ^{1}H isotope abundance H_2O (Barnstead E-Pure, 18 MΩ)/D_2O/0.1 M potassium phosphate buffer.

Solution pH was measured using a standardized, calibrated Fisher combination electrode and an Orion Model 310 meter and in D_2O solutions is reported as pH′, indicating the meter reading without adjustment for the deuterium isotope effect. Minor adjustments to CcP solution pH were made using DCl, NaOD, and D_3PO_4 (all Isotec). However, the pH titrations presented in this work necessitated repetitive gentle pH changes of 1−2 mM enzyme solutions, which were carried out by cycles of dilution in the desired buffer followed by concentration to ∼0.5 mL for NMR, employing Centricon concentrators (Amicon).

NMR experiments were carried out using a Varian Inova spectrometer operating at the nominal proton frequency of 500 MHz. Proton spectra were all processed using line broadening apodization equivalent to 5−20 Hz (1D spectra) and combinations of Gaussian and shifted Gaussian apodization in 2D spectra. Both 1D and 2D spectra were processed *without* using any type of baseline straightening procedure; hence some of the baselines in the spectra of Figures 3−10 appear slightly curved. Observed proton chemical shifts were internally referenced to the residual HDO peak, which was assigned a shift of 4.70 ppm at 21 °C and neutral pH. Several types of homonuclear proton two-dimensional experiments were carried out including Clean TOCSY (*38*), NOESY (*39*), and WET-NOESY (*40*), in which off-resonance water suppression was implemented using a WET sequence. WET-1D and standard S2PUL experiments were also employed. NMR data were processed on an O_2 computer (Silicon Graphics Inc.) using VNMR software (Varian, Inc.) and were edited for publication using Photoshop 4.0 (Adobe Systems). Protein Data Bank (PDB) coordinate files of X-ray crystal structures of natWTCcP (PDB code 2CYP; *28*), rCcP(MI,-H52L) (PDB code 5CCP; *10*), and natWTCcPCN, the coordinates of which were a gift from Prof. Thomas L. Poulos, University of California, Irvine, were processed, edited, and plotted on a Power Macintosh G3 computer using WebLab Viewer Lite (Accelrys) and then further edited using Photoshop 4.0 (Adobe Systems).

An estimate of the equilibrium chemical exchange rate in rCcP(H52L) was made from the ^{1}H NMR data using the pairs of heme methyl resonances that are apparently interconverting (8/f and e/1 in Figure 5), using a method described in ref *57*. This estimate involves making several assumptions of varying accuracy and validity. These are (a) that the enzyme is in "slow exchange" at 34 and 30 °C, but it is in "no exchange" at 21 °C, (b) that the values of the no-exchange, 21 °C, shifts for peak pairs 8/f and e/1 (Figure 5) can be obtained from extrapolation of the variable temperature shift data, and (c) that the peak positions for the overlapped pairs can be accurately interpolated. In this system a large error is introduced by further assuming that variable temperature shifts are due only to dynamic exchange. Since values of T_2 could not be independently measured for rCcP-(H52L) due to resonance overlap, estimates were made for T_2 values of 2 and 5 ms. The calculated exchange rates ranged from 787 to 1123 s^{-1} for the four calculated cases. Averaging the four values gave 1004 s^{-1}. So an "average" estimate of 1000 s^{-1} is deemed reasonable, given all of the caveats and assumptions.

RESULTS AND DISCUSSION

CcP Structural References. For the sake of clarity in the following discussion of NMR data, we present in Figure 1

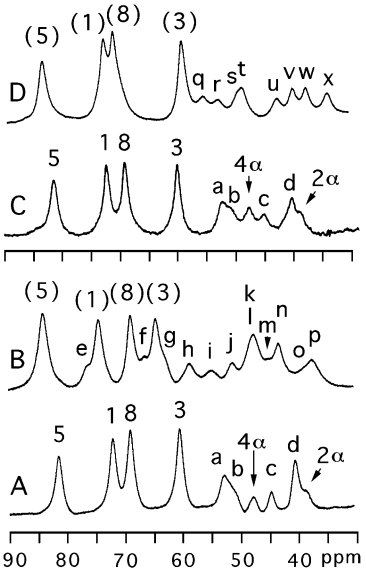

FIGURE 3: High-frequency region, hyperfine-shifted ^{1}H NMR spectra (500 MHz; 21 °C) of the resting states of (A) rCcP, 99.9% D_2O/0.1 M potassium phosphate, pH′ = 7.2, (B) rCcP(H52L), 99.9% D_2O/0.1 M potassium phosphate, pH′ = 7.4, (C) natWTCcP, 99.9% D_2O/0.3 M potassium nitrate, pH′ = 7.1, and (D) rCcP-(H52L), 99.9% D_2O/0.3 M potassium nitrate, pH′ = 6.9. Assignments are labeled in (A) and (C). Tentative assignments are shown in parentheses in (B) and (D). Spectra were acquired using WET-1D and were processed without baseline straightening.

the heme *b* structure, which we use with Fischer system labeling. We also present edited views of the heme pockets of crystal structures of natWTCcP (2CYP; *8*, *28*), CcP(MI,H52L) (5CCP; *10*), and natWTCcPCN (no PDB code). The rCcP(H52L) used in this work contains the exact primary sequence as natWTCcP (2CYP) and the previously described rCcP (*30*), except for the noted point mutation. Previous work (*10*, *11*) employed a His52 variant whose sequence differed from natWTCcP and rCcP by containing an N-terminal extension consisting of Met-Ile and mutations at positions 53 and 152 [CcP(MI,H52L); *41*, *42*]. Companion kinetic studies have revealed identical kinetic constants for rCcP(H52L) and CcP(MI,H52L) (*27*). The parent sequence of this recombinant CcP has been called CcP(MI) to signify these sequence differences (*41*, *42*). Characterizations of CcP(MI) have revealed only minor structural and functional differences compared to natWTCcP (*41*, *42*). Therefore, we believe that direct comparisons between the spectroscopic work described here for natWTCcP, rCcP, and rCcP(H52L) and previously published work on CcP(MI) and CcP(MI,H52L) are valid.

Resting-State Enzyme: Solution Composition. Proton NMR spectra of the hyperfine shift regions of resting-state (i.e., high spin, ferriheme) forms of the CcPs used in this work are shown in Figure 3. Figure 3A shows that rCcP, the recombinant wild-type enzyme, displays an NMR spectrum that is identical to that of yeast-isolated natWTCcP (Figure 3C; *30*) and for which the high-frequency region (12−82 ppm) consists of 10 discernible resonances. The four previously assigned (*43*) heme methyl peaks are labeled 5, 1, 8, and 3 in Figures 1A and 2A,C. Two additional single proton resonances (2α vinyl, 4α vinyl) are also labeled (*43*). Of the four unassigned resonances remaining in this region, peaks labeled a and d each have relative integrated intensities corresponding to at least two protons, while peaks labeled b and c correspond to single protons. These unassigned proton resonances must be due to the four propionate α protons (Figure 1A) and the two diastereotopic β-CH_2 protons of the heme-coordinating proximal histidine (His175; Figure 1B). There is no evidence in the spectra of Figure 3A,C or in the spectra of yeast-isolated natWTCcP (*17*, *30*, *43*, *44*) of more than one form of the enzyme in solution at pH 6−8, at temperatures below 30 °C (*43*, *44*).

In contrast, spectra of rCcP(H52L) in identical solution conditions to rCcP reveal evidence of at least two enzyme forms simultaneously in solution, as shown in Figure 3B. Instead of 10 discernible resonances Figure 3B shows 16 peaks and shoulders, labeled (5), (1), (8), (3), and e−p. Although no specific resonances have been experimentally assigned for rCcP(H52L), there is clearly a set of major resonances consisting of the four most prominent peaks that must be the heme methyl resonances of the major form. We suggest tentative individual assignments for these four, noted in parentheses in Figure 3, on the basis of correspondence with the spectra in Figure 3A,C. No direct resonance assignments have been made in rCcP(H52L) due to the extensive resonance overlap, which has rendered 1D NOE experiments and magnetization exchange experiments impossible and, also as a result of the enzyme instability, which has confounded heme reconstitution experiments.

Single proton resonances of this major form are to be found among the more intense of the remaining group (probably peaks h, i, j, k, l, n, and p). The combined peak, labeled k, l consists of at least two resonances, discernible due to the pronounced peak asymmetry. One of the peaks among those labeled e, f, g may also belong to the major enzyme form. However, the remaining two of those, along with peaks m and o and small shoulders on peaks h and i, constitute the resonances of at least one minor enzyme form. Due to the large resonance line widths and concomitant lack of resolution, it is likely that additional minor form peaks are hidden under the major form resonances.

When the solution salt composition is changed to 0.3 M KNO_3 from 0.1 M potassium phosphate, the rCcP(H52L) spectrum changes to a single set of resolved resonances (Figure 3D). Four proposed heme methyl resonance assignments are shown in parentheses and are based on assignments in natWTCcP in KNO_3 (*43*). There is, additionally, a set of eight unassigned single proton resonances labeled q−x that are fully or partially resolved, corresponding exactly to the sum of the four heme α-propionate protons, the two heme α-vinyl protons, and the two hyperfine-shifted His175 βCH_2 protons, as for rCcP and natWTCcP (Figure 1B).

Figure 3 is important because it demonstrates that in solutions of rCcP(H52L) at least two distinct enzyme forms are detected by proton NMR spectroscopy. Appearance of the minor form(s) occurs in 0.1 M potassium phosphate buffer but not in 0.3 M KNO_3 salt solution. Therefore, the minor form's presence is a function of the solution composition and may be related either to specific NO_3^- binding (*24*) or by specific PO_4^{3-} binding, which has not yet been demonstrated for CcP. Although this assessment is not comprehensive, it is important for the reason that it establishes that at least two enzyme forms coexist in solutions of resting-state rCcP(H52L). The solution heterogeneity is not due to impure enzyme preparations. The preparations of this enzyme were shown to be pure by several biochemical

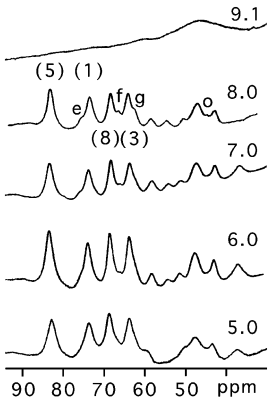

FIGURE 4: High-frequency region, hyperfine-shifted ^{1}H NMR spectra (500 MHz; 21 °C; 90% H_2O/10% D_2O/0.1 M potassium phosphate) of resting-state rCcP(H52L) at several pHs. Tentative heme methyl resonance assignments are in parentheses. Spectra were acquired using WET-1D and were processed without baseline straightening.

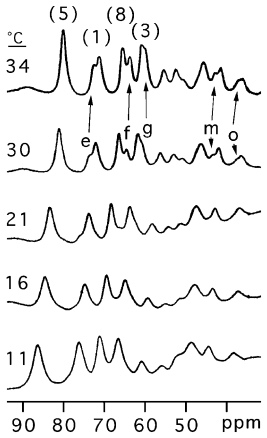

FIGURE 5: High-frequency region, hyperfine-shifted ^{1}H NMR spectra (500 MHz; pH′ = 7.8; 99.9% D_2O/0.1 M potassium phosphate) of resting-state rCcP(H52L) at several temperatures. Tentative heme methyl resonance assignments are in parentheses. Spectra were acquired using WET-1D and were processed without baseline straightening.

assessments, include PAGE, which showed a single line, MALDI-TOF mass spectrometry, typical of a single protein as previously shown for other CcP preparations (*30*, *45*), and plasmid sequencing.

Resting-State rCcP(H52L): pH Behavior. We previously studied the solution pH behavior of natWTCcP by proton NMR in the range pH′ = 8 to pH′ = 4.5 (*44*). That work employed KNO_3 solutions and showed that there are acid and neutral forms of CcP that interconvert with an apparent pK = 5.6. The proton hyperfine spectra of the two forms are quite different (*43*, *44*).

Figure 4 shows that the hyperfine proton resonances of rCcP(H52L) in 90% H_2O/0.1 M potassium phosphate buffer also have pH-dependent observed shifts, particularly obvious among the single proton resonances in the 40−55 ppm region. They tend toward coalescence at ∼48 ppm at pH = 5.0. Even at this low pH, however, the four heme methyl resonances remain well defined, in contrast to natWTCcP in KNO_3 solution, and there is no evidence in rCcP(H52L) of a new set of methyl resonances that would indicate the previously detected pK = 5.6 transition (*44*). This is consistent with an expected pK_a shift to lower pH previously identified in studies of CcP salt dependence (*10*, *15*, *20*, *24*−*26*). At higher pH there is evidence of a minor form that develops prominence in the interval pH 6−8. This second form becomes more apparent in variable temperature studies (vide infra) and will be further described in that context.

At high pH (pH = 9.1) the high-frequency hyperfine shift spectrum degrades to a single broad resonance. This reflects the high pH transition described in our companion paper (*27*). The broadness and lack of definition in the pH = 9.1 spectrum indicate either loss of heme active site structural integrity or increased active site dynamics, or both. This is consistent with optical studies that reveal complex kinetics above pH 8 (*11*, *27*). The observed ^{1}H shift of the broad resonance at pH 9 and above is consistent with optical and Raman studies that have shown that resting CcP converts to low-spin (OH-ligated) forms at alkaline pH (*10*, *11*, *15*).

Resting-State rCcP(H52L): Temperature Dependence. Varying temperature has three effects on the ^{1}H spectrum of high-spin rCcP(H52L), as shown in Figure 5. (i) Due to heme paramagnetism the hyperfine resonances display a general Curie law effect (*46*) with observed shifts increasing as the temperature is lowered. (ii) In addition, the increasing solution viscosity at lower temperatures causes the resonances to broaden, whereas they narrow significantly as the temperature is raised. At 34 °C it appears as if the putative 1-CH_3, 8-CH_3, and 3-CH_3 resonances are composed of nearly equal doublets. (iii) Tracing the appearance and development of the "minor" (e, f, g) resonances of these doublets from the 21 °C spectrum reveals that as the temperature rises they gain intensity relative to the 21 °C major form resonances. This is illustrated nicely by the minor peak labeled e, which is merely a high-frequency shoulder on the proposed 1-CH_3 resonance at 21 °C but develops into a peak of nearly equal intensity by 34 °C.

The experiment shown in Figure 5 was reversible. This behavior indicates a temperature-dependent equilibrium interconversion between major and minor enzyme forms. From the pattern of observed resonance doubling it is reasonable to assign the low-temperature minor form peaks labeled e, f, g, respectively, to 1-CH_3, 8-CH_3, and 3-CH_3 resonances in this minor form. The low-temperature minor form and major form resonances for the proposed 5-CH_3 are completely coincident over this temperature range, as indicated by the fact that the integrated peak intensity corresponds to the sum of any of the other methyl resonance "doublets". Temperature-dependent changes can also be seen in the complement of single proton resonances but are not uniquely interpretable due to peak broadness and the high degree of resonance overlap in the 30−60 ppm region.

Summary of HS rCcP(H52L) Results. These studies of high-spin, 5-coordinate, resting-state rCcP(H52L) have identified an equilibrium mixture of at least two enzyme forms in the purified enzyme preparation. Their temperature-dependent interconversion (Figure 5) is reversible, indicating the presence of a dynamic equilibrium between enzyme forms, which favors an apparent single form at low temperature (low pH) and favors a different form at high temperature (high pH). Identification of this heterogeneity raises two important issues: (i) whether, and to what extent, this heterogeneity manifests itself in the CN-ligated variant and (ii) whether the two enzyme forms affect ligand binding kinetics. As shown in the following sections, ^{1}H NMR

Table 1: Heme Hyperfine ^{1}H Shifts (in ppm) and Assignments for WTCcPCN and [H52L]CcPCN at 21 °C, in 99% D_2O or 90% H_2O, at pH′ 7.0 and 10.4

peak no.	heme assignment	WTCcPCN, 99% D_2O, pH′ 7.0	H52L-CN, 99% D_2O, pH′ 7.0	H52L-CN, 90% H_2O, pH′ 7.0	WTCcPCN, 99% D_2O, pH′ 10.4	H52L-CN, 99% D_2O, pH′ 10.4
1″			29.2	29.4		
1	8CH_3	30.8	28.5	28.6	28.8	29.3
1′			27.4	27.9		
3′			26.8	27.0		
3	3CH_3	27.7	26.3	26.7	26.0	25.8
3″				26.3		
4′			18.9	18.9		
4	His175 β-H	19.5	18.6	18.6	20.2	20.8
5	7-αH	18.3	17.5	17.4	17.9	18.2
8	4-αH	16.0	15.5	15.4	15.1	15.3
9′			14.8			
9	His175 β-H*	14.9	14.5			
10	His52 C_ϵ-H	14.0				
11	His175 NpH	12.8				

spectra of rCcP(H52L)CN reveal greater heterogeneity than could be detected in spectra of the resting state.

The kinetic analysis described in the accompanying paper (*27*) rationalizes the (NMR detectable) two forms [labeled E, E′ for HS rCcP(H52L)] by requiring their equilibrium interconversion to be fast compared to the rate of cyanide binding, while the NMR spectra (Figure 5) show two enzyme forms that are in slow exchange on the NMR time scale. These are not incompatible requirements. It is not possible to make precise measurements of equilibrium exchange rates for rCcP(H52L) from NMR spectra (Figure 5) because of the severe hyperfine-shifted resonance overlap, the inappropriate ^{1}H T_2 of the heme resonances, and the limited window of temperature stability in which the two enzyme forms are resolved. However, a less precise, qualitative estimate for the exchange rate is 1000 s^{-1} (see Experimental Procedures). Therefore, while slow by NMR criteria, this equilibrium exchange is fast compared to the fastest pseudo-first-order CN on-rate determined by stopped-flow kinetics, which is 10 s^{-1} (see ref *27*).

rCcP(H52L)CN: Solution Heterogeneity. Spectroscopic changes (UV−visible, NMR) reveal that both CcP and rCcP(H52L) bind cyanide to form the corresponding low-spin enzyme forms, which are also paramagnetic but are physiologically inactive. The refined structure coordinates of natWTCcPCN are available (Figure 1C), based on an earlier published structure (*47*). No structure of rCcP(H52L)CN has yet been reported. Figure 6 compares the 1D ^{1}H NMR spectra of rCcPCN and rCcP(H52L)CN in 99.9% D_2O/0.1 M potassium phosphate buffer (Figure 6A,B) and in 90% H_2O/10% D_2O/0.1 M potassium phosphate buffer (Figure 6C,D). Assignments and definition of resonance labels for the numbered resonances in Figure 6A,C have been made using experiments described here and by analogy to a database of assignments for rCcPCN (*45*), natWTCcPCN (*32*−*36*), and several variants (*17*, *48*−*50*). These are given in Table 1.

We anticipate these results because Figure 6 clearly indicates that, in comparison to rCcPCN (and natWTCcPCN; *34*, *35*), the rCcP(H52L)CN proton NMR spectrum consists of multiple sets of hyperfine resonances. This result indicates that the mutant enzyme has a highly heterogeneous active site.

The spectra shown in Figures 6−10 indicate that four identifiable enzyme forms are present in millimolar solutions

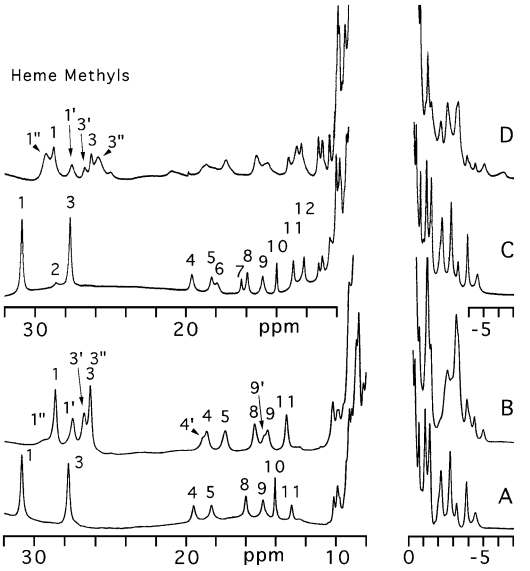

FIGURE 6: Proton hyperfine resonance shift regions at 500 MHz (21 °C) of (A) rCcPCN, 99.9% D_2O/0.1 M potassium phosphate, pH′ = 7.4, (B) rCcP(H52L)CN, 99.9% D_2O/0.1 M potassium phosphate, pH′ = 7.4, (C) rCcPCN, 90% H_2O/10% D_2O/0.1 M potassium phosphate, pH′ = 7.8, and (D) rCcP(H52L)CN, 90% H_2O/10% D_2O/0.1 M potassium phosphate, pH′ = 7.8. Spectra were acquired with WET-1D, so that partial saturation of the isotope exchangeable peaks (peaks 2, 6, and 7) occurs in (C). All spectra were processed without baseline straightening. Peak assignments corresponding to numbered resonances are given in Table 1.

of rCcP(H52L)CN. In keeping with similar work (*17*, *48*−*50*), we label the resonances in these various enzyme forms as follows. Unprimed labels (i.e., peaks numbered 1, 3) indicate resonances of the low-temperature major enzyme form. Double primed labels (i.e., 1″, 3″) indicate the high-temperature predominant form. Primed labels (i.e., 1′, 3′) and triple-primed labels (i.e., 1‴, 3‴) indicate the third and fourth (respectively) enzyme forms. [Note: E, E′ for HS rCcP(H52L) and E, E′ for LS rCcP(H52L)CN are not the same.] In most of our spectra (Figures 6−10) the magnetically distinguishable resonances of enzyme forms E, E′, and E″ are easily observed. However, in the contour plot in Figure 7A and in the resolution-enhanced 2D-sum projection spectrum shown in Figure 7B, we can also identify two additional resonances (peaks labeled 1‴, 3‴) constituting a fourth enzyme form. These resonances occur as barely

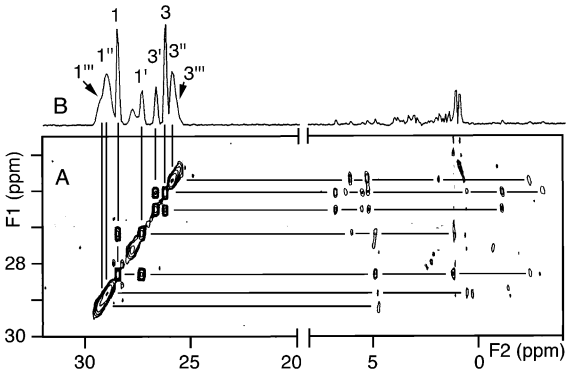

FIGURE 7: (A) A section of the full ^{1}H WET-NOESY (40 ms mix) contour plot for rCcP(H52L)CN (24 °C, 99.9% D_2O/0.1 M potassium phosphate, pH′ = 7.4) showing correlations with the downfield pairs of heme methyl resonances. Chemical exchange cross-peaks are apparent among the methyl resonances in the 25−28 ppm region. (B) Sum projection plotted on the same shift scale. Spectra were processed without baseline straightening.

resolved shoulders on peaks 1″ and 3″, respectively, and typically overlap those of 1″ and 3″ in one-dimensional spectra. Due to limitations of spectral resolution, data for the fourth form are limited, but for the other three enzyme forms our data (Figures 9 and 10) show that all three forms are interconverted by temperature, pH, and solvent isotope composition (H_2O vs D_2O), as described in the following.

Our labeling scheme is further illustrated by focusing on the heme methyl shift region where peaks labeled 1 (8-CH_3) and 3 (3-CH_3) occur, at 25−31 ppm in Figure 6 (Table 1). When rCcP(H52L)CN is in 99.9% D_2O buffer (Figure 6B), there are two prominent, narrow heme methyl resonances (peaks 1 and 3) with two pairs of smaller, broader resonances overlapping them (peaks labeled 1′, 3′ and 1″, 3″). However, when rCcP(H52L)CN is in 90% H_2O buffer (Figure 6D), the relative intensities of these peaks have changed significantly, indicating that the relative amount of the low-temperature minor enzyme form, 1″/3″ (and probably 1‴ and 3‴), has increased relative to the predominant enzyme form in D_2O buffer, (1/3). Further details concerning the interconversion of these enzyme forms will become obvious in the discussion of Figures 7−9.

Comparing the (H52L)CcPCN and rCcPCN spectra (Figure 6) further reveals that the His52 C_ϵ-H hyperfine resonance (peak 10 in Figure 6A,C) found in rCcPCN and natWTCcPCN (*33*−*36*, *44*, *45*) is absent in the rCcP(H52L)CN spectrum (Figure 6B,D), an expected result of the His52 → Leu replacement. This confirms the mutation and also the key observation that His52 protons are hyperfine shifted in spectra of natWTCcPCN and rCcPCN. Observation of three His52 hyperfine-shifted proton resonances in rCcPCN spectra, in 90% H_2O buffer (peaks 2, 7, and 10 in Figure 6C; *33*−*35*), emphasizes the presence of a hydrogen bond between His52 and heme-coordinated CN in the native enzymes. Anticipating later results, we propose that His52 hydrogen bonding is a seminal component in preserving the active site dynamic and structural chemistry of CcP.

CN-Ligated Enzymes: Assignments and Dynamics. Beginning with initially proposed hyperfine resonance assignments for rCcP(H52L)CN derived from comparisons with our CcPCN database, we carried out ^{1}H NOESY and TOCSY experiments to confirm or refine those initial proposals (Table 1). Examples of the NOESY data are shown in Figures 7 and 8. From experiments such as these it was possible to sort out some of the overlapping hyperfine-shifted resonances and make low-level rCcP(H52L)CN assignments by proton type such as those shown in Figures 7 and 8. Making further specific resonance assignments is more complicated than will be described here due to the multiple species in solution, and this work remains in progress.

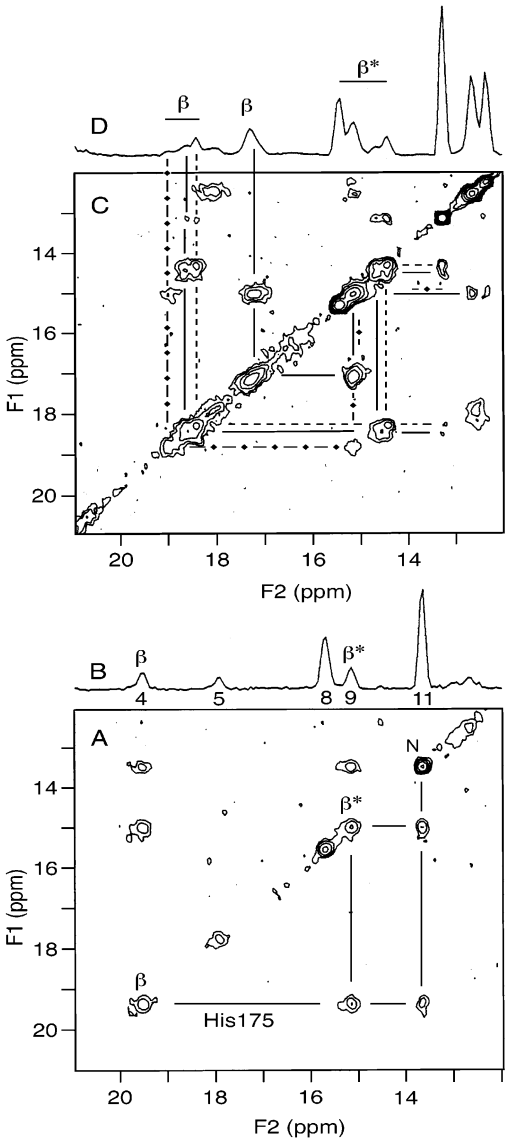

FIGURE 8: (A) Section of the full ^{1}H WET-NOESY (40 ms mix) contour plot for rCcP(H52L)CN in 99.9% D_2O/0.1 M potassium phosphate, pH′ = 7.4, at 11 °C, showing the single set of His175 cross-peaks from the major low-temperature enzyme form. (B) Sum projection of the NOESY spectrum in (A). (C) Section of the full ^{1}H WET-NOESY (15 ms mix) contour plot that is identical for (A), for rCcP(H52L)CN in 99.9% D_2O/0.1 M potassium phosphate, pH′ = 7.4, at 24 °C, showing the multiple sets of what are apparently His175 cross-peaks. (D) Sum projection of the NOESY spectrum in (C). Spectra were processed without baseline straightening.

These experiments also established the dynamic interconversion between forms E and E′ as shown by the 1/1′ and 3/3′ exchange cross-peaks in the heme methyl region (25−31 ppm) in Figure 7A. Observation of chemical exchange cross-peaks supports the mechanism proposed in the accompanying paper (*27*) to account for the observed kinetics in terms of the NMR-detectable multiple enzyme forms. Only

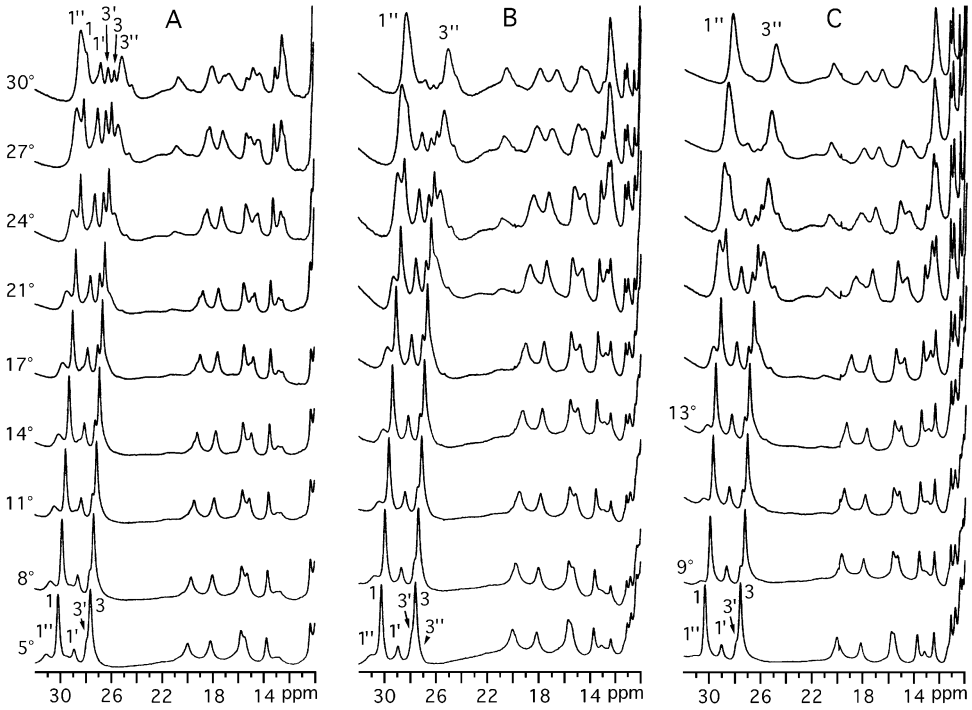

FIGURE 9: ^{1}H high-frequency hyperfine-shifted region of rCcP(H52L)CN NMR spectra as a function of temperature in three different solvent isotope compositions: (A) 99.9% D_2O/0.1 M potassium phosphate, pH′ = 7.4; (B) 50% D_2O/50% H_2O/0.1 M potassium phosphate, pH′ = 7.6; (C) 90% H_2O/10% D_2O/0.1 M potassium phosphate, pH = 7.8. Spectra were processed without baseline straightening.

these two cross-peaks were observed due to the overlap among the other heme methyl resonances.

Figure 7 also helped to establish the bona fide nature of all four enzyme forms in the following way. The horizontal lines in Figure 7A delineate a complicated set of cross-peaks showing that separate cross-peak arrays can be defined for all of these four pairs of heme methyl resonances. Only the array associated with peak 3‴ is not well resolved due to its overlap with the 3″ resonance.

Resolution of four enzyme species is also seen in 2D plots of the single proton hyperfine shift region (21−12 ppm). Figure 8A shows a ^{1}H NOESY (40 ms mixing time) spectrum plotted at the noise baseline level for rCcP(H52L)-CN in 99.9% D_2O buffer at 11 °C, where the E form predominates (as in Figure 9A). Peaks 4, 9, and 11 shown in the projection in Figure 8B correspond (*32*−*36*) to the following three separate proximal histidine (His175) protons: the geminal βH pair (peaks 4 and 9) and the peptide NH (peak 11). At this comparatively long mixing time the following cross-peaks are observed, as traced on the spectrum: βH/βH*, βH*/NH, and βH/NH. In CcPCN His175 cross-peaks are the only ones that occur in the hyperfine shift region shown in this figure under these conditions (*32*−*36*). At 24 °C in the same buffer at the same pH, several additional sets of cross-peaks are found in this region, as shown in Figure 8C. These result from increasingly populating the minor forms of the enzyme at higher temperatures (see Figure 9A), which is also illustrated by the appearance of additional resonances in the one-dimensional projection shown in Figure 8D (compare to Figure 9A).

Figure 8C was obtained at a shorter mixing time (15 ms) than Figure 8A (40 ms) in order to reduce the complexity of the cross-peak identification problem. However, it is similarly plotted at the noise baseline. Reducing the mixing time reduces all cross-peak intensities but in this case nearly eliminates all βH/NH cross-peaks in this region, simplifying the analysis. In Figure 8C the most intense cross-peaks are from the (diastereotopic) geminal βH/βH* and βH*/NH connectivities. The lines drawn on the figure trace out four sets of connected cross-peaks, some of which overlap. These define four sets of what are apparently the His175 βH/βH*/NH resonances corresponding to four different enzyme forms. Consistent with this interpretation is heterogeneity in the single proton, broad, low-frequency His175 peak (not shown), which is split into two main resonances (−21.4 and −24.0 ppm at 21 °C), each asymmetrical, and includes an identifiable shoulder at −20.3 ppm.

What is interesting about these spectra is the fact that the four NMR-distinguishable enzyme forms in rCcP(H52L)-CN are detected via protons that lie in both equatorial (heme methyl resonances) and axial (His175 resonances) regions of the heme paramagnetic field. These results are therefore due to structural differences propagated comprehensively throughout the active sites of each form, or they reflect altered heme electronic structures, or both. The latter could be caused by changes in the axial ligand field strength, which is suggested by the variation in line widths of the heme methyl resonances of the four forms (Figures 7B, 9, and 10).

CN-Ligated Enzymes: Temperature and Solvent Isotope Effects. The dynamic nature of the E/E′/E″ (and presumably E‴) interconversions is further illustrated in Figure 9, which shows the combined effects of altering temperature and solvent isotope composition (H_2O vs D_2O). The general trend in these spectra is that, whether in D_2O/0.1 M potassium phosphate buffer or H_2O/0.1 M potassium phosphate buffer, at low temperatures (below 24 °C in D_2O, pH′ = 7.4; below 17 °C in H_2O, pH = 7.8), there is a predominant form (E) represented by the 8-CH_3 (peak 1), and 3-CH_3 (peak 3) resonances. At 5 °C there are only small amounts of the minor forms (E′, E″) present as indicated by the smaller 1′/

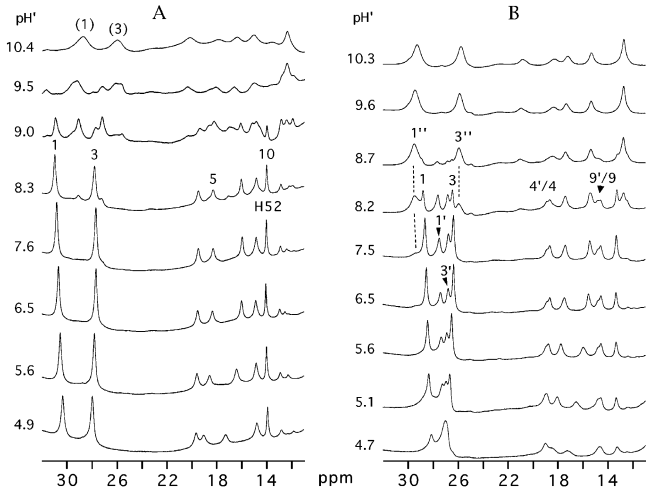

FIGURE 10: (A) pH dependence of rCcPCN and (B) rCcP(H52L)-CN, represented by high-frequency ^{1}H hyperfine-shifted NMR spectra (500 MHz, 21 °C, 99.9% D_2O/0.1 M potassium phosphate). Spectra were processed without baseline straightening.

3′ and 1″/3″ resonances. Below 17 °C the spectra are not significantly dependent on the solvent isotope composition. However, above 17 °C the spectra are dramatically dependent on whether the buffer solution was 99.9% D_2O, 90% H_2O, or a mixture of the two. At 17 °C and higher, peaks of the E″ form increase in relative intensity in all of the solvent systems and reach almost exclusive predominance in 90% H_2O buffer at 30 °C, the highest temperature examined. At 30 °C there may also be contributions from the E‴ form; however, this form cannot be independently resolved due to resonance overlap with the E″ form resonances and their comparable line widths. The trend reflected in the Figure 9 spectra is that the relative concentration of the low-temperature major form, E, decreases with respect to both E′ and E″ as temperature increases. At highest temperature E″ (E‴) predominates.

CN-Ligated Enzymes: pH Dependence. As shown in Figure 10, the resolved hyperfine ^{1}H spectrum of rCcP-(H52L)CN also undergoes complex pH-linked changes. The lowest pH spectrum (Figure 10B; pH′ = 4.7) reveals much broader resonances than rCcPCN (Figure 10A; pH′ = 4.9) and an unusual heme methyl resonance pattern in which both 1′ and 3′ methyl resonances collapse to overlap with peak 3. As the pH is raised, these two resonances emerge from the overlap and resolve individually. Up to pH′ = 6.5 resonances from E and E′ are the only ones obvious. At pH′ = 6.5 and above the E″ heme methyl resonances increase in relative intensity and by pH′ above ~8.7 are the sole heme methyl resonances, indicating that E″ (E‴) is at least 90% of the enzyme form in solution.

CN-Ligated Enzymes: His52 Titration. The data in Figure 10A (see also ref *31*) allow us to associate the pH-dependent, NMR-detected transition above pH′ = 8.3 (in D_2O buffer) for natWTCcPCN with titration of His52 in the following way. The spectrum of natWTCcPCN presented in Figure 10A shows only minor changes from pH′ = 4.9 to pH′ = 8.3. At pH′ = 8.3 one can see minor-form peaks surrounding the heme 3-CH_3 (peak 3) at 28.8 and 27.0 ppm. As pH increases there is a clear transition involving intermediate forms, typified by multiple overlapped resonances, until a single set of broader resonances emerges and predominates by pH′ = 10.4 (*31*). During this transition the His52 $C_\epsilon H$ (peak 10) resonance is lost from the hyperfine spectrum, indicating that the hydrogen bond between His52 and heme-bound CN has been disrupted. As expected, no similar shift transition is seen for rCcP(H52L)CN (Figure 10B).

In fact, the rCcP(H52L)CN spectrum at pH′ = 10.3 and the natWTCcPCN spectrum at pH′ = 10.4 are remarkably similar to each other, both in pattern and in the larger line widths in both spectra compared to their respective neutral pH/low-temperature forms (Figures 9 and 10). The pH-dependent transformation of rCcP(H52L)CN to the high-pH form (Figure 10B) involves continuous conversion through the NMR-identifiable minor forms as the pH increases. The transition is essentially complete by pH′ = 8.7. In contrast, for rCcPCN (Figure 10A) essentially a single enzyme form is observed up to pH′ = 8.3. At higher pH a dramatic spectral conversion occurs, where at pH′ = 9.0 and 9.5 one can count at least eight principal individual resonances in the heme methyl resonance region (30−24 ppm). If they are heme methyl resonances, which occur in pairs in this region, it indicates the presence of at least four magnetically distinct enzyme forms in rCcPCN, albeit in only a small pH range. These forms appear in concert with the disappearance of the His52 $C_\epsilon H$ resonance, resulting from pH titration of His52 that eliminates it as a hydrogen bond donor to heme-coordinated CN. The parallel to rCcP(H52L)CN is striking. The pH transition for rCcPCN is complete by pH′ = 10.4, about 1.7 pH units more basic than for rCcP(H52L)CN.

The spectra in Figure 10 reveal that in rCcPCN there are two related high-pH processes. One represents transition to an alkaline form whose ^{1}H hyperfine NMR spectrum is characterized by broad resonances that are spectrally similar to the rCcP(H52L)CN alkaline form. The accompanying process, specific to rCcPCN, is the alkaline titration of His52, resulting in loss of the His52 $C_\epsilon H$ proton resonance (peak 10) from the hyperfine-shifted spectrum. The spectrum showing multiple solution forms for rCcPCN at pH′ 9.5 (Figure 10A) is similar to various spectra of rCcPCN(H52L), for example, Figure 6D, Figure 9A−C (above 21°), and Figure 10B (at pH 8.2). This titration was previously observed for natWTCcPCN, although it could not be interpreted because that study preceded definitive hyperfine ^{1}H resonance assignments (*31*).

Two other conclusions derived from Figure 10 bear mentioning. (i) For rCcPCN, peak 5 exhibits titration behavior identical to natWTCcPCN (*31*). This peak is one of the (diastereotopic) heme 7-propionate geminal αH pairs (Figure 1A). Since propionate-7 is hydrogen bonded to His181, its pH sensitivity indicates alteration in this bond, which likely results from titration of His181. This identifies His181 as a likely candidate for one of the two protons in the CcP acid−alkaline transition (*15*, *18*−*21*, *51*−*53*). (ii) The heterogneity in His175 resonances is further demonstrated by the apparent doubling of the His175 geminal pair of β protons (peaks 4/4′ and 9/9′) in Figures 6 and 10B. This heterogeneity is resolved by pH′ = 5.1 and persists above pH′ = 8.2. We note that heterogeneity has also been observed in the Fe−ligand Raman bands in the analogous low-spin CcPCO(MI,H52L) (*15*). Two to three protein species were differentiated in this structurally analogous reduced enzyme form.

CN-Ligated Enzymes: His52 and Active Site Integrity. In native forms of CcPCN, His52 participates in two hydrogen bonds via both of its imidazole ring nitrogens (N_δ and N_ϵ), indicated in Figure 2C. His52 N_δH hydrogen bonds to Asn82 (which in turn hydrogen bonds to Glu76), whereas N_ϵH hydrogen bonds to heme-bound CN, as previously described (*33*, *34*, *49*, *50*). Appearance of interconvertible multiple enzyme forms for several CcP mutants is clearly correlated with disruption of His52 hydrogen-bonding ability (*48*−*50*). Multiple enzyme forms, observed here, resulting from the His52 → Leu mutation extend those previous observations.

Similar NMR studies with HRPCN, a related peroxidase, revealed corresponding chemistry involving its distal histidine, His42 (*30*, *54*, *55*), which corresponds to His52 in CcP. In HRPCN His42 also hydrogen bonds to heme-bound cyanide (*30*, *54*, *55*). Since the number of HRP variants examined by NMR to date is less than for CcP, comparisons are necessarily less extensive. However, distal amino acid mutations similar to those engineered into CcP (*48*−*50*) were found to similarly disrupt kinetics and hydrogen bonding in HRP and HRPCN (*54*, *55*). For example, NMR spectra of HRPCN(N70D) show evidence of multiple enzyme forms (*55*), as do spectra of the corresponding CcPCN(N82D) (*49*). However, NMR spectra of the CcP variant are much more highly affected, as previously discussed (*49*, *50*, *55*). These examples exemplify the principal hydrogen-bonding role of peroxidase distal histidines from two species. This may be a general property required for proper peroxidase function. In CcP this role is implied to also be independent of heme ligand identity, since infrared studies of natWTCcPCO provided additional evidence that His52 hydrogen bonds to heme-bound CO (*56*). Such observations strengthen the chemical relevance of our presumptive use of HCN binding as a surrogate for H_2O_2 binding and the structural model analogues presented in Figure 2.

There are also differences between the data reported here and other data reported for both peroxidases. Alkaline titration of His52 in natWTCcPCN shown in Figure 10 is reportedly not observed for the structurally related, reduced enzyme, CcPCO(MI,H52L) (*15*). It is also reported not to occur for HRPCN (*37*). Those two reports concluded that His52 is not involved in the alkaline transition, whereas for CcPCN it obviously plays a role.

Implications for the CcP Mechanism. The distal histidine's hydrogen-bonding role in CcPCN (and HRPCN) is precisely the His52 function envisioned by mechanisms of CcP's enzymic cycle (*2*, *8*, *11*, *22*), as illustrated in Figure 2B. On the basis of the structural models in Figure 2, demonstrated hydrogen bonding by His52 in CcPCN, the anticipated chemical similarities between the CcPCN and CcP−ES active sites, and the observation of multiple forms of rCcP(H52L) and rCcP(H52L)CN (vide supra), the data presented here suggest that His52 plays a fundamental structural role in CcP catalysis (*2*, *8*, *10*, *11*, *21*, *22*). Erman and co-workers have made a detailed study of how the His52 → Leu substitution in CcP(MI) affects the kinetics of its oxidation by H_2O_2 and a peroxy acid, *p*-nitroperoxybenzoic acid (pNPBA) (*11*, *22*). CcP(MI) reacts with H_2O_2 to form compound I about 2.6 times faster than with pNPBA at pHs where both oxidants exist primarily in their protonated, neutral forms (*11*, *22*). They formulated four microscopic steps that, in turn, constitute the bimolecular oxidation reaction mechanism and concluded that the rate-determining step is diffusion of the oxidant through the protein matrix (*22*). The His52 → Leu substitution in CcP(MI,H52L) decreased the rate of the oxidation reaction for both neutral oxidants (H_2O_2, pNPBA) by about 5 orders of magnitude. Similarly, they found that the anion of pNPBA ($pNPBA^-$) reacted about 3 orders of magnitude more slowly with CcP(MI,H52L) than with natWTCcP. The authors reasoned that in CcP−ES (Figure 2B) His52 hydrogen bonds to the heme-bound −O−OH, utilizing one of the protons conveyed to the heme pocket by the neutral peroxide, HOOH. This is the origin of the concept of a base catalysis role for His52 in the decomposition of hydrogen peroxide (*2*, *8*, *11*, *22*). In reactions with the anion, $pNPBA^-$, which does not convey a labile proton to the active site, structures such as that shown in Figure 2B could not occur, implying no kinetic advantage for nativelike CcPs containing His52 and a H52L variant. The prediction of nearly equal rates for the initial oxidation reaction of $pNPBA^-$ with both natWTCcP and CcP(MI,H52L) was not observed (*11*). The 3 orders of magnitude decrease in the rate of reaction of the pNPBA anion in rCcP(H52L) compared to natWTCcP lead Erman et al. (*11*, *22*) to conclude that "...the distal histidine has a more complex role than base catalysis to promote binding to the heme iron", since it is unlikely that the pNPBA anion would require base catalysis to react rapidly with the heme iron.

We note in the accompanying paper (*27*) that, in reactions with cyanide ion at alkaline pH that do not require a proton, the rates of reaction for rCcP(H52L) and rCcP are comparable. This indicates that hydrogen bonding is not required for cyanide ion binding to CcP. Further analyses of the kinetic data in the accompanying paper (*27*) suggest that the hydrogen- bonding role of His52 is for assisting dissociation of H_2O_2 in compound ES (Figure 2B) and heme-coordinated cyanide (Figure 2C).

The "more complex" role envisaged for His52 may also involve stabilizing a single reactive form of resting-state CcP. In the absence of the stabilizing interaction(s), as in rCcP(H52L), multiple forms of CcP exist, which contribute to the kinetics of hydrogen cyanide binding (*8*, *27*) and presumably to peroxide binding. Why the different forms of rCcP(H52L) have different reactivity is still an open question, but it may involve access to the heme iron, since substitution of the distal histidine by a nonpolar residue, such as leucine, also alters the polarity of the heme group and the electrostatic interactions in the heme pocket. This can alter the arrangement of active site water molecules in the resting-state enzyme and affect access of charged reactants, such as the cyanide ion at higher pH.

Origin of Variant Enzyme Forms. The NMR data indicate that dynamic interconversion occurs between the multiple enzyme forms of rCcPCN(H52L), dependent upon pH, temperature, and solvent isotope composition. This suggests that it is an active site multistructural phenomenon involving the well-defined hydrogen-bonding network and including active site water molecules, as previously discussed (*50*).

ACKNOWLEDGMENT

J.D.S. gratefully acknowledges Drs. Harold Goldberg, Michael Kwasman, Lawrence Hammond, and Stacey Dean, whose compassion, talent, and expertise made this paper

possible. We thank Professor Thomas Poulos, University of California, Irvine, for kindly making available to us plasmid pT7CCPZf1 and the X-ray crystal coordinates of CcPCN.

REFERENCES

1. Dunford, H. B. (1999) *Heme Peroxidases*, J. Wiley and Sons, New York.
2. Bosshard, H. R., Anni, H., and Yonetani, T. (1991) in *Peroxidases in Chemistry and Biology* (Everse, J., Everse, K. E., and Grisham, M. B., Eds.) Vol. 2, pp 52−78, CRC Press, Boca Raton, FL.
3. Everse, J., Everse, K. E., and Grisham, M. B., Eds. (1990) *Peroxidases in Chemistry and Biology*, Vols. I and II, CRC Press, Boca Raton, FL.
4. English, A. M., and Tsaprailis (1995) *Adv. Inorg. Chem. 43*, 79−125.
5. Poulos, T. L. (1988) *Adv. Inorg. Biochem. 7*, 1−36.
6. Mauro, J. M., Miller, M. A., Edwards, S. L., Wang, J., Fishel, L. A., and Kraut, J. (1989) in *Metal Ions in Biological Systems* (Sigel, H., and Sigel, A., Eds.) Vol. 25, pp 477−503, Marcel Dekker, New York.
7. Charizanis, C., Juhnke, H., Krems, B., and Entian, K. D. (1999) *Mol. Gen. Genet. 262* 437−447.
8. Poulos, T. L., and Kraut, J. (1980) *J. Biol. Chem. 255*, 8199−8205.
9. Miller, M. A. (1996) *Biochemistry 35*, 15791−15799.
10. Erman, J. E., Vitello, L. B., Miller, M. A., Shaw, A., Brown, K. A., and Kraut, J. (1993) *Biochemistry 32*, 9798−9806 (Protein Data Bank crystal structure ID: 5CCP).
11. Palamakumbura, A. H., Vitello, L. B., and Erman, J. E. (1999) *Biochemistry 38*, 15653−15658.
12. Vitello, L. B., Erman, J. E., Miller, M. A., Wang, J., and Kraut, J. (1993) *Biochemistry 32*, 9807−9818.
13. Miller, M. A., Vitello, L., and Erman, J. E. (1995) *Biochemistry 34*, 12048−12058.
14. Millett, F., Miller, M. A., Geren, L., and Durham, B. (1995) *J. Bioenerg. Biomembr. 27*, 341−351.
15. Smulevich, G., Miller, M. A., Kraut, J., and Spiro, T. G. (1991) *Biochemistry 30*, 9546−9558.
16. Bonagura, C. A., Sundaramoorthy, M., Pappa, H., Patterson, W., and Poulos, T. L. (1996) *Biochemistry 35*, 6107−6115.
17. Satterlee, J. D., Erman, J. E., Mauro, J. M., and Kraut, J. (1990) *Biochemistry 29*, 8797−8804.
18. Conroy, C. W., and Erman, J. E. (1978) *Biochim. Biophys. Acta 527*, 370−378.
19. Kang, D. S., and Erman, J. E. (1982) *J. Biol. Chem. 257*, 12775−12779.
20. Erman, J. E. (1974) *Biochemistry 13*, 39−44.
21. Loo, S., and Erman, J. E. (1975) *Biochemistry 14*, 3467−3470.
22. Palamakumbura, A. H., Foshay, M. C., Vitello, L. B., and Erman, J. E. (1999) *Biochemistry 38*, 15647−15652.
23. Banci, L., and Pierattelli, R. (1999) *Spectrochim. Acta 55A*, 415−420.
24. Vitello, L. B, Huang, M., and Erman, J. E. (1990) *Biochemistry 29*, 4283−4288.
25. Vitello, L. B., Erman, J. E., Mauro, J. M., and Kraut, J. (1990) *Biochim. Biophy. Acta 1038*, 90−97.
26. Vitello, L. B., Erman, J. E., Miller, M. A., Mauro, J. M., and Kraut, J. (1992) *Biochemistry 31*, 11524−11535.
27. Bidwai, A., Witt, M., Foshay, M., Vitello, L. B., Satterlee, J. D., and Erman, J. E. (2003) *Biochemistry 42*, 10764−10771.
28. Finzel, B. C., Poulos, T. L., and Kraut, J. (1984) *J. Biol. Chem. 259*, 13027−13036 (Protein Data Bank crystal structure ID: 2CYP).
29. Erman, J. E., and Vitello, L. B. (1998) *J. Biochem. Mol. Biol. 31*, 307−327.
30. Teske, J. G., Savenkova, M. I., Mauro, J. M., Erman, J. E., and Satterlee, J. D. (2000) *Protein Expression Purif. 19*, 139−147.
31. Satterlee, J. D., and Erman, J. E. (1983) *J. Biol. Chem. 258*, 1050−1056.
32. Satterlee, J. D., Erman, J. E., La Mar, G. N., Smith, K. M., and Langry, K. C. (1983) *J. Am. Chem. Soc. 105*, 2099−2104.
33. Satterlee, J. D., Erman, J. E., and de Ropp, J. S. (1987) *J. Biol. Chem. 262*, 11578−11583.
34. Satterlee, J. D., and Erman, J. E. (1991) *Biochemistry 30*, 4398−4405.
35. Satterlee, J. D., Russell, D. J., and Erman, J. E. (1991) *Biochemistry 30*, 9072−9077.
36. Banci, L., Bertini, I., Turano, P., Ferrer, J. C., and Mauk, A. G. (1991) *Inorg. Chem. 30*, 4510−4516.
37. Thanabal, V., de Ropp, J. S., and La Mar, G. N. (1988) *J. Am. Chem. Soc. 110*, 3027−3035.
38. Griesinger, C., Otting, G., Wuthruch, K., and Ernst, R. R. (1988) *J. Am. Chem. Soc. 110*, 7870−7872.
39. Kumar, A., Ernst, R. R., and Wuthrich, K. (1980) *Biochem. Biophys. Res. Commun. 95*, 1−7.
40. Smallcombe, S. H., Patt, S. L., and Keifer, P. A. (1995) *J. Magn. Reson., Ser. A 117*, 295−303.
41. Fishel, L. A., Villafranca, J. E., Mauro, J. M., and Kraut, J. (1987) *Biochemistry 26*, 351−360.
42. Wang, J., Mauro, J. M., Edwards, S. L., Oatley, S. J., Fishel, L. A., Ashford, V. A., Xuong, N.-H., and Kraut, J. (1990) *Biochemistry 29*, 7160−7173.
43. Satterlee, J. D., Erman, J. E., La Mar, G. N., Smith, K. M., and Langry, K. C. (1983) *Biochim. Biophys. Acta 743*, 246−255.
44. Satterlee, J. D., and Erman, J. E. (1980) *Arch. Biochem. Biophys. 202*, 608−616.
45. Savenkova, M. I., Satterlee, J. D., Erman, J. E., Siems, W. F., and Helms, G. L. (2001) *Biochemistry 40*, 12123−12131.
46. La Mar, G. N., Satterlee, J. D., and de Ropp, J. S. (2000) in *The Porphyrin Handbook* (Kadish, K. M., Smith, K. M., and Guilard, R., Eds.) Vol. 5, pp 185−298, Academic Press, San Diego.
47. Poulos, T. L., Freer, S. T., Alden, R. A., Xuong, N.-H., Edwards, S. L., Hamlin, R. C., and Kraut, J. (1978) *J. Biol. Chem. 253*, 3730−3735.
48. Satterlee, J. D., Alam, S. L., Mauro, J. M., Erman, J. E., and Poulos, T. L. (1994) *Eur. J. Biochem. 224*, 81−87.
49. Alam, S. L., Satterlee, J. D., Mauro, J. M., Poulos, T. L., and Erman, J. E. (1995) *Biochemistry 34*, 15496−15503.
50. Satterlee, J. D., Teske, J. G., Erman, J. E., Mauro, J. M., and Poulos, T. L. (2000) *J. Protein Chem. 19*, 535−542.
51. Conroy, C. W., Tyma, P., Daum, P. H., and Erman, J. E. (1978) *Biochim. Biophys. Acta 537*, 62−69.
52. Miller, M. A., Coletta, M., Mauro, J. M., Putnam, L. D., Farnum, M. F., Kraut, J., and Traylor, T. G. (1990) *Biochemistry 29*, 1777−1791.
53. Miller, M. A., Mauro, J. M., Smulevich, G., Coletta, M., Kraut, J., and Traylor, T. G. (1990) *Biochemistry 29*, 9978−9988.
54. Tanaka, M., Nagano, S., Ishimori, K., and Morishima, I. (1997) *Biochemistry 36*, 9791−9798.
55. Nagano, S., Tanaka, M., Ishimori, K., Watanabe, Y., and Morishima, I. (1996) *Biochemistry 35*, 14251−14258.
56. Satterlee, J. D., and Erman, J. E. (1984) *J. Am. Chem. Soc. 106*, 1139−1140.
57. Martin, M. L., Delpuech, J. J., and Martin, G. J. (1980) *Practical NMR Spectroscopy*, Chapter 8, Heyden & Son, London.

BI034633C